IJC Heart & Vasculature 37 (2021) 100897

Contents lists available at ScienceDirect

IJC Heart & Vasculature

journal homepage: www.sciencedirect.com/journal/ijc-heart-and-vasculature

Left ventricular vortex analysis by high-frame rate blood speckle tracking echocardiography in healthy children and in congenital heart disease

Pietro Marchese [a,b], Massimiliano Cantinotti [a], Jef Van den Eynde [c,d], Nadia Assanta [a], Eliana Franchi [a], Vitali Pak [a], Giuseppe Santoro [a], Martin Koestenberger [e], Shelby Kutty [c,*]

[a] Fondazione G. Monasterio CNR-Regione Toscana, Massa and Pisa, Italy
[b] Adult Institute of Clinical Physiology, Pisa, Italy
[c] Taussig Heart Center, Department of Pediatrics, Johns Hopkins Hospital, Baltimore, MD, USA
[d] Department of Cardiovascular Sciences, KU Leuven, Leuven, Belgium
[e] Division of Pediatric Cardiology, Medical University Graz, Austria

ARTICLE INFO

Keywords:
Blood speckle imaging
Heart defects
Congenital
Echocardiography
Left ventricle
Pediatrics
Vortex imaging

ABSTRACT

Background: High-frame rate blood speckle tracking (BST) echocardiography is a new technique for the assessment of intracardiac flow. The purpose of this study was to evaluate the characteristics of left ventricular (LV) vortices in healthy children and in those with congenital heart disease (CHD).
Methods: Characteristics of LV vortices were analyses based on 4-chamber BST images from 118 healthy children (median age 6.84 years, range 0.01–17 years) and 43 children with CHD (median age 0.99 years, range 0.01–14 years). Both groups were compared after propensity matching. Multiple linear regression was used to identify factors that independently influence vortex characteristics.
Results: Feasibility of vortex imaging was 93.7% for healthy children and 95.6% for CHD. After propensity matching, there were no overall significant differences in vortex distance to apex, distance to interventricular septum (IVS), height, width, sphericity index, or area. However, multiple regression analysis revealed significant associations of LV morphology with vortex characteristics. Furthermore, CHD involving LV volume overload and CHD involving LV pressure overload were both associated with vortices localized closer to the IVS.
Conclusions: LV vortex analysis using high-frame rate BST echocardiography is feasible in healthy children and in those with CHD. As they are associated with LV morphology and are modified in some types of CHD, vortices might yield diagnostic and prognostic value. Future studies are warranted to establish applications of vortex imaging in the clinical setting.

1. Introduction

High-frame rate Blood speckle tracking (BST) echocardiography is a new technique for the assessment of blood flow.[1–7] BST may be used to visualize and quantify intra- and extra-cardiac flow patterns, and could improve our understanding of cardiac physiology. Compared to conventional Doppler, high-frame-rate BST is an ultrafast technique which generates up to thousands of frames per second and which is independent of the angle of insonation.[1–2]

Blood flow in the cardiovascular system occurs in different ways including laminar, turbulent, or vortical flow. The latter is described as a circular or swirling motion. Vortices naturally form in all cardiac chambers, but have been studied most extensively in the left ventricle (LV).[1,2,7] They represent a reservoir of kinetic energy in the LV,

Abbreviations: AV, atrioventricular; BMI, body mass index; Bpm, beats per minute; BSA, body surface area; BST, blood speckle tracking; CHD, congenital heart disease; CI, correlation index; ED, end-diastolic; Fps, frame per second; -i, indexed to BSA; ICC, intraclass correlation coefficient; IQR, interquartile range; IVS, interventricular septum; LV, left ventricle/ventricular; LVEDA, left ventricular end-diastolic area; LVEDD, left ventricular end-diastolic dimension; LVEDV, left ventricular end-diastolic volume; LVEF, left ventricular ejection fraction; LVESD, left ventricular end-systolic dimension; LVESV, left ventricular end-systolic volume; LVOT, left ventricular outflow tract; LVPO, CHD involving left ventricle pressure overload; LVSV, left ventricular stroke volume; LVVO, CHD involving left ventricular volume overload; MV, mitral valve; RVPO, CHD involving right ventricular pressure overload; RVVO, CHD involving right ventricular volume overload; TGA, transposition of the great arteries.

* Corresponding author at: Johns Hopkins Hospital and School of Medicine, 1800 Orleans St, Baltimore, MD 21287, USA.
E-mail address: skutty1@jhmi.edu (S. Kutty).

https://doi.org/10.1016/j.ijcha.2021.100897
Received 15 August 2021; Received in revised form 14 October 2021; Accepted 15 October 2021

facilitating systolic ejection of blood flow into the left ventricular outflow tract (LVOT). It has been demonstrated in adults how the geometry and anatomical locations of vortices differ in health and disease. [2,5–7] Therefore, vortex analysis may represent a novel and promising index of LV dysfunction.

Data on intracardiac vortices in healthy children are limited,[1,8] and studies on LV vortex formation in children with congenital heart disease (CHD) are lacking. BST has been technically validated in pediatric patients, but its clinical applications need to be further explored. [3–6] The aim of the present investigation was to evaluate the presence and characteristics of LV vortices in healthy children and in those with CHD.

2. Methods

2.1. Study population

This study conforms to the ethical guidelines of the 1975 Declaration of Helsinki as reflected in a priori approval by the Local Ethics Committee of the Fondazione CNR-Regione Toscana G. Monasterio of Massa (Study "Bet" N.390). Healthy Caucasian children (<18 years old) were prospectively recruited from May 2020 to November 2020 in the outpatient Pediatric Cardiology Department at the Fondazione CNR-Regione Toscana G. Monasterio of Massa. Neonates and infants were evaluated for "innocent murmurs" while older children and young adolescents were evaluated as part of sports screening. Healthy subjects were defined as those without clinical, electrocardiographic, or echocardiographic evidence of CHD or acquired heart disease. Exclusion criteria for the group of healthy subjects were: (1) known or suspected neuromuscular disease, genetic syndromes, or chromosomal abnormalities; (2) body mass index (BMI) $\geq$ 95th percentile for children $\geq$ 2 years old or weight-for-length Z-score $\geq$ 2 based on the World Health Organization (WHO) Child Growth Standards for children < 2 years old;[9] (3) pulmonary hypertension;[9] (4) systemic hypertension in children > 4 years of age; (5) connective tissue disease; or (6) family history of genetic cardiac disease such as Marfan syndrome or cardiomyopathy.[9] In addition, a group of children with CHD undergoing complete echocardiographic examination were included. Parents or legal guardians of all the children accepted to participate in the study by signing a written informed consent.

CHD was classified as follows: (a) LVPO: CHD involving left ventricle pressure overload, including aortic stenosis, aortic coarctation, and bicuspid aortic valve; (b) LVVO: CHD involving left ventricular volume overload, including ventricular septal defect, atrioventricular septal defect, patent ductus arteriosus, and aorto-pumonary window; (c) RVPO: CHD involving right ventricular pressure overload, including tetralogy of Fallot, pulmonary stenosis, and pulmonary atresia; (d) RVVO: CHD involving right ventricular volume overload, including atrial septal defect); (e) transposition of the great arteries (TGA); and (f) other types of CHD.

2.2. Echocardiography examinations

All patients underwent a complete 2-dimensional echocardiographic examination. Images were collected only in quiet and cooperative children. Infants could bottle feed and older children could watch cartoons during the examinations. No child was sedated.

Echocardiographic examinations were performed using a Vivid E 95system (GE Ultrasound) with 12 (4–12 MHz) and 6S (2.7–8.0 MHz) probe (GE Healthcare). BST imaging was obtained from a focused and zoomed view of the LV in apical 4-chamber view incorporating the entire LV including the interventricular septum and mitral valve annulus.[8,10] The color Doppler sector with BST analysis was positioned over the LV and a clip of at least 2 cardiac cycles at a range of 380 frames per second (fps) with Nyquist limits ranging from 53 to 58 cm/s were acquired. Images were digitally stored for subsequent offline analysis, which was performed directly on the machine, to evaluate the presence, number, and characteristics of LV vortices.

The following vortex characteristics were measured from frozen images: position, height (mm), width (mm), sphericity index, and area (cm^2). Position of the vortex was calculated in relation to two lines: (1) a line from the ventricular apex to the mitral valve, and (2) a line from the IVS to the LV free wall. Vortex height was determined by measuring the longitudinal dimension of the main vortex relative to LV length, and vortex width as the horizontal dimension of the vortex relative to LV width. Sphericity Index was defined as the ratio of vortex height/width. [1] When the main vortex was visible over several phases of the cardiac cycle, measurements were made for each phase and the phase where the vortex had the biggest dimension was selected for the final analysis. Vortex dimensions were indexed by body surface area (BSA)[11] and LV end-diastolic area (LVEDA) on apical 4 chamber view.[12] The absence of a clean-edged vortex was considered as an exclusion criterion. Vortices at the level of the mitral valve annulus were also excluded since they usually had poor reproducibility.

2.3. Statistical analyses

Continuous variables were checked for normality using the Shapiro-Wilk test. Normally distributed variables are presented as mean $\pm$ SD and were compared using the student *t*-test; non-normally distributed variables are presented as median (interquartile range, IQR) and were compared using Mann-Whitney *U* test. Categorical variables are expressed as frequency (%) and were compared with the Chi-squared test. To account for baseline differences between groups, age-matched pairs were obtained using the nearest neighbor method via the R package "MatchIt" (version 4.1.0.). Multiple linear regression models were generated to identify factors that independently influence vortex position and dimension. Eligible variables included any of those listed in Table 1. Starting from the null model, variables were introduced in a stepwise fashion based on the Akaike Information Criterion (AIC) and age was forced in all models. All models were created using the R package "MASS" (version 7.3–53.1) and were checked for overfitting. Before creating the regression models, missing data were imputed using distributive imputation via the R package "mice" (version 3.13.0). Intra- and inter-rater reliability was assessed using intra-class correlation coefficients (ICC). Intra-rater reliability was defined as the degree of agreement among repeated measurements on the same BST scan performed by a single rater, while inter-rater reliability was defined as the extent to which two independent raters agree. All analyses were performed using R Statistical Software (version 4.0.5, Foundation for Statistical Computing, Vienna, Austria). A two-tailed p-value < 0.05 was considered statistically significant.

3. Results

3.1. Study population and feasibility

A total of 171 subjects including 126 healthy children and 45 children with CHD (median age 6.31 years, IQR 0.93–10.2 years) were recruited. Ten subjects were excluded due to the failure to achieve a clean-edged vortex within the permissible transducer depth of field (Fig. 1). Therefore, feasibility was 93.7% for healthy children and 95.6% for those with CHD. Patients who were excluded did not differ significantly from those included in the study (Table 1).

As a result, data from 161 children were available for analysis, including 118 healthy children and 43 children with various types of CHD (Fig. 1). Participant characteristics are presented in Table 1. All participants had normal LV systolic function. Among children with CHD, 23 (53.5%) had a history of surgical or percutaneous intervention. In both groups, optimal vortex visualization was achieved at a Nyquist limit between 53 and 58 cm/s.

As the group with CHD was significantly younger at the time of

Table 1
Participant characteristics.

Variable	Included (n = 161)					Excluded (n = 10)	
	Healthy children before matching (n = 118)	Healthy children after matching (n = 43)	Children with CHD (n = 43)	P-value healthy vs CHD before matching	P-value healthy vs CHD after matching	Children excluded from study (n = 10)	P-value included vs excluded
Age, years	6.84 (2.94–10.5)	1.53 (0.37–6.84)	0.99 (0.10–6.82)	<0.001	0.473	3.34 (0.91–4.64)	0.441
Male sex	67 (56.8%)	21 (48.8%)	35 (81.4%)	0.007	0.001	6 (60.0%)	0.830
Anthropometric data							
Height, cm	121 (89.2–142)	80.0 (62.5–114)	75.0 (58.5–116)	<0.001	0.613	97.5 (71.0–115)	0.267
Weight, kg	25.0 (14.3–37.2)	11.0 (6.55–24.0)	7.95 (4.22–19.0)	<0.001	0.327	18.0 (8.88–20.8)	0.459
BMI, kg/m^2	17.3 (15.6–19.0)	16.9 (15.8–18.5)	14.6 (13.5–16.8)	<0.001	<0.001	16.6 (16.0–17.4)	0.197
BSA, m^2	0.92 (0.60–1.22)	0.52 (0.34–0.87)	0.41 (0.26–0.78)	<0.001	0.383	0.71 (0.42–0.81)	0.881
HR, bpm	90.0 (79.0–111)	114 (87.5–148)	110 (89.0–144)	0.002	0.870	/	/
SBP, mmHg	106 (101–114)	101 (95.0–111)	98.5 (85.0–108)	0.001	0.066	/	/
DBP, mmHg	60.9 ± 8.50	61.0 (8.49)	57.1 ± 12.4	0.105	0.164	/	/
ΔBP, mmHg	46.5 ± 10.5	42.2 (7.68)	38.7 ± 13.6	0.003	0.211	/	/
Cardiac morphology and function							
LVEDV, mL	53.0 (28.0–71.6)	21.0 (13.0–53.4)	21.0 (10.0–49.5)	<0.001	0.520	/	/
LVEDVi, mL/m^2	54.7 (43.1–61.6)	42.9 (35.1–53.7)	42.9 (33.3–58.4)	0.007	0.897	/	/
LVESV, mL	19.0 (11.0–29.1)	9.00 (4.76–18.2)	6.51 (3.50–16.0)	<0.001	0.327	/	/
LVESVi, mL/m^2	20.0 (16.9–25.2)	17.8 (12.8–21.1)	16.3 (9.56–20.9)	0.002	0.302	/	/
LVSV, mL	32.5 (18.0–42.1)	13.0 (8.00–33.0)	14.0 (5.50–28.4)	<0.001	0.653	/	/
LVSVi, mL/m^2	32.9 (26.1–39.3)	25.0 (22.3–32.8)	26.7 (20.9–35.2)	0.008	0.816	/	/
LVEF, %	61.0 (57.5–66.0)	62.8 (57.0–67.0)	64.0 (57.1–71.0)	0.189	0.257	/	/
LVEDA, cm^2	19.2 (12.5–24.4)	10.4 (7.58–19.1)	10.5 (6.70–19.0)	<0.001	0.854	/	/
LVEDAi, cm^2/m^2	20.9 (18.8–22.8)	21.3 (19.3–23.5)	21.5 (19.3–25.0)	0.108	0.437	/	/
LVEDD, mm	59.9 (49.5–68.4)	44.0 (37.0–58.5)	45.0 (35.5–57.5)	<0.001	0.697	/	/
LVEDD/BSA, mm/m^2	64.9 (55.6–82.8)	83.6 (68.4–110)	95.6 (65.9–126)	<0.001	0.288	/	/
CHD-related characteristics							
History of surgical or percutaneous intervention	/		23 (53.5%)	/		/	/
Type of CHD							
LVPO	/		19 (44.2%)	/		/	/
LVVO	/		8 (18.6%)	/		/	/
RVPO	/		9 (20.9%)	/		/	/
RVVO	/		1 (2.3%)	/		/	/
TGA	/		3 (7.0%)	/		/	/
Other CHD	/		3 (7.0%)	/		/	/

BMI = body mass index; bpm = beats per minute; BSA = body surface area; CHD = congenital heart diseases; DBP = diastolic blood pressure; ΔBP = difference between systolic and diastolic blood pressure; HR = heart rate; LV = left ventricular; LVEDA = left ventricular end-diastolic area; LVEDD = left ventricular end-diastolic dimension; LVEDV = left ventricular end-diastolic volume; LVEF = left ventricular ejection fraction; LVESV = left ventricular end-systolic volume; LVPO = CHD involving left ventricle pressure overload (including aortic stenosis, aortic coarctation, and bicuspid aortic valve); LVSV = left ventricular stroke volume; LVVO = CHD involving left ventricular volume overload (including ventricular septal defect, atrioventricular septal defect, patent ductus arteriosus, and aorto-pumonary window); RVPO = CHD involving right ventricular pressure overload (including tetralogy of Fallot, pulmonary stenosis, and pulmonary atresia); RVVO = CHD involving right ventricular volume overload (including atrial septal defect); TGA = transposition of the great arteries; -i = indexed to BSA.

echocardiographic examination (0.99, IQR 0.10–6.82 versus 6.84, IQR 2.94–10.5, $p < 0.001$) and because age has an important influence on cardiac dimensions, 43 age-matched pairs were obtained using propensity score matching. Both matched groups were comparable with regard all baseline characteristics, although there remained a significantly higher proportion of male participants (83.7% versus 48.8%, $p = 0.001$) and a lower BMI (14.6, IQR 13.5–16.8 versus 16.9, IQR 15.8–18.5, $p < 0.001$) in the CHD group (Table 1).

3.2. Vortex imaging

In most children (147, 91.3%) only a single vortex was observed, while 2 were observed in 9 children (5.6%, 7 healthy children and 2 with CHD), 3 in 4 children (2.5%, 2 healthy children and 2 with CHD), and 4 in 1 child with CHD (0.6%). Only a limited number of vortices were found in the systolic phase of the cardiac cycle, including 27 in healthy children and 12 in those with CHD; therefore, analysis of vortex characteristics was performed only for vortices presenting in the diastolic

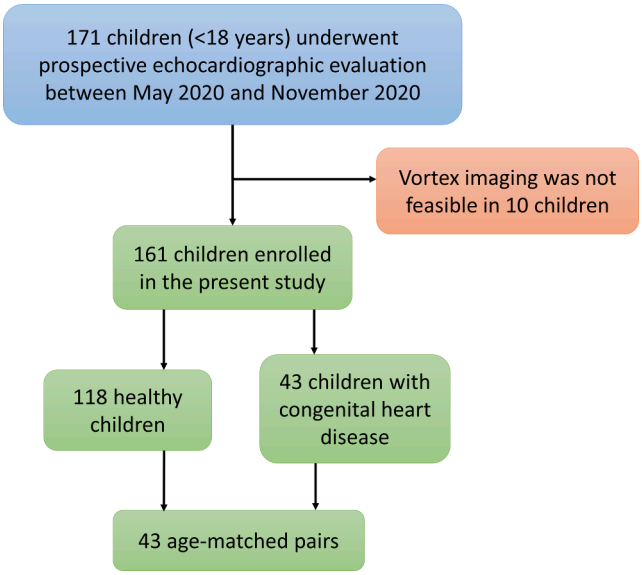

Fig. 1. Flow chart of the study population.

phase. The diastolic phase was divided based on electrocardiography tracing into three phases: early, mid, and late diastole. In 18 healthy children (15.3%) the main vortex could be visualized throughout all three diastolic phases, while in 45 (38.1%) it could be traced only in two consecutive phases. In the remainder, the main vortex was observed only in early diastole (34, 28.8%), mid diastole (11, 9.3%), or late diastole (10, 8.5%). In the CHD group, the main vortex was followed along all three phases of diastole in 11 children (25.6%), while only in two consecutive diastolic phases in 16 (37.2%). In the remainder, the main vortex was visualized only in early diastole (7, 16.3%), mid diastole (4, 9.3%), or late diastole (5, 11.6%).

3.3. Vortex characteristics

Characteristics of the main vortex are summarized in Table 2. The main vortex was observed in the mid-septal region of the LV in all subjects. In the unmatched cohorts, the distance of the vortex to the apex and to the IVS was significantly shorter in patients with CHD (all $p < 0.05$); however, this difference disappeared when these distances were divided by the distance from apex to mitral valve ($p = 0.655$) and from IVS to LV free wall ($p = 0.712$), respectively (Table 2). After matching, there was no longer a difference between the distances to the apex ($p = 0.126$) or IVS ($p = 0.338$) of both groups.

The biggest dimensions for each vortex were mainly seen either in early or late diastole (84.8% in healthy children and 74.4% in children with CHD). In the unmatched analysis, Sphericity Index was similar between both groups ($p = 0.597$). Similarly, the groups did not differ with regard to vortex height ($p = 0.477$), width ($p = 0.629$), or area ($p = 0.192$) (Table 2). Contrastingly, when indexed to BSA, these dimensions were all significantly larger in the CHD group (all $p < 0.001$). When indexed to LVEDA, patients with CHD had significantly smaller vortex height and width (both $p < 0.001$) and larger area ($p = 0.005$). However, these differences disappeared after matching (all $p > 0.05$).

3.4. Regression models

The previous results suggested no differences in vortex characteristics between healthy children and children with CHD in propensity-matched analyses, with differences in the unmatched analyses related to the younger age in the CHD group. Therefore, multiple regression models were applied to the full study population to further investigate factors that might influence vortex characteristics. Significant independent predictors of vortex distance to apex/distance from apex to mitral valve, distance to IVS/distance from IVS to LV free wall, height/LVEDA, width/LVEDA, sphericity, and area/LVEDA are listed in Table 3. The complete regression models are given in Supplemental Material, Table S1.

No significant predictors of vortex distance to the apex were found. In contrast, it was observed that having any type of CHD was associated with larger distances to the IVS, whereas neonates, LVPO, and LVVO were associated with significantly smaller distances to the IVS.

Vortex height/LVEDA increased with increasing body weight and LV end-diastolic dimension indexed to BSA (LVESDi), while it decreased with increasing body height, BMI, LVEDA indexed to BSA (LVEDAi), and LV end-diastolic dimension indexed to BSA (LVEDDi). Similarly, vortex

Table 2
Vortex characteristics.

Variable	Healthy children before matching (n = 118)	Healthy children after matching (n = 43)	Children with CHD (n = 43)	P-value healthy vs CHD before matching	P-value healthy vs CHD after matching
Vortex position					
Distance to apex, mm	21.2 (16.0–28.0)	17.9 (13.7–21.0)	16.5 (12.1–23.9)	0.001	0.766
Distance to apex/distance from apex to mitral valve, %	39 (32–49)	38 (30–51)	39 (30–48)	0.655	0.742
Distance to IVS, mm	11.0 (8.42–13.5)	9.41 (6.49–13.4)	8.70 (6.10–13.3)	0.041	0.526
Distance to IVS/distance from IVS to LV free wall, %	31 (25–41)	37 (27–45)	34 (25–40)	0.712	0.309
Vortex dimensions					
Phase of the cardiac cycle at which the biggest vortex was measured				0.239	0.904
Early diastole	61 (51.7%)	16 (37.2%)	17 (39.5%)		
Mid diastole	18 (15.3%)	10 (23.3%)	11 (25.6%)		
Late diastole	39 (33.1%)	17 (39.5%)	15 (34.9%)		
Height, mm	9.41 (7.80–11.0)	9.24 (6.69–10.7)	8.82 (7.32–10.8)	0.447	0.586
Height/BSA, mm/m^2	10.7 (7.95–15.4)	15.3 (10.3–20.5)	18.6 (11.4–28.3)	<0.001	0.142
Height/LVEDA, mm/cm^2	0.75 (0.54–1.31)	0.74 (0.50–1.03)	0.51 (0.40–0.73)	<0.001	0.429
Width, mm	7.45 (6.19–9.24)	6.86 (5.63–8.24)	7.12 (6.03–9.46)	0.629	0.254
Width/BSA, mm/m^2	9.18 (6.86–11.9)	12.4 (9.25–15.6)	16.7 (10.2–22.5)	<0.001	0.051
Width/LVEDA, mm/cm^2	0.66 (0.48–0.98)	0.57 (0.44–0.81)	0.43 (0.34–0.57)	<0.001	0.235
Sphericity Index	1.20 (1.05–1.39)	1.24 (1.06–1.50)	1.18 (1.00–1.33)	0.597	0.437
Area, cm^2	0.60 (0.42–0.80)	0.50 (0.30–0.69)	0.49 (0.37–0.78)	0.192	0.666
Area/BSA, cm^2/m^2	0.67 (0.51–0.95)	0.82 (0.63–1.08)	1.01 (0.75–1.64)	<0.001	0.096
Area/LVEDA, cm^2/cm^2	0.03 (0.02–0.05)	0.04 (0.03–0.06)	0.04 (0.03–0.08)	0.005	0.349

BSA = body surface area; CHD = congenital heart diseases; IVS = interventricular septum; LV = left ventricular; LVEDA, left ventricular end-diastolic area.

Table 3
Significant independent predictors of vortex characteristics in multiple linear regression.

Independent variables	Beta	SE	t-statistic	p-value
Dependent variable: Distance to IVS/distance from IVS to LV free wall, %				
CHD	0.090	0.035	2.562	0.011
LVPO	−0.089	0.041	−2.176	0.031
LVVO	−0.112	0.053	−2.090	0.038
Neonates	−0.129	0.049	−2.643	0.009
Dependent variable: Vortex height/LVEDA, mm/cm^2				
Neonates	0.342	0.138	2.481	0.014
Weight, kg	0.067	0.021	3.173	0.002
Height, cm	−0.016	0.008	−2.116	0.036
BMI, kg/m^2	−0.082	0.020	−4.153	<0.001
LVESDi, mm/m^2	0.005	0.002	2.833	0.005
LVEDAi, cm^2/m^2	−0.005	0.002	−3.087	0.002
LVEDDi, mm/m^2	−0.013	0.003	−5.186	<0.001
Dependent variable: Vortex width/LVEDA, mm/cm^2				
Neonates	0.354	0.094	3.783	<0.001
Weight, kg	0.055	0.014	3.873	<0.001
Height, cm	−0.015	0.005	−2.952	0.004
BMI, kg/m^2	−0.067	0.013	−5.144	<0.001
LVEDAi, cm^2/m^2	−0.004	0.001	−3.537	0.001
LVEDDi, mm/m^2	−0.010	0.002	−5.824	<0.001
Dependent variable: Sphericity Index				
LVEDVi, mL/m^2	−0.159	0.069	−2.285	0.024
LVESVi, mL/m^2	0.154	0.068	2.267	0.025
LVSVi, mL/m^2	0.164	0.071	2.299	0.023
LVESDi, cm^2/m^2	0.003	0.001	3.085	0.002
Dependent variable: Vortex area/LVEDA, cm^2/cm^2				
Weight, kg	0.006	0.001	4.004	<0.001
BMI, kg/m^2	−0.003	0.001	−3.004	0.003
BSA, m^2	−0.265	0.059	−4.455	<0.001
LVEDAi, cm^2/m^2	−0.001	0.001	−2.023	0.045
LVEDDi, mm/m^2	−0.001	0.000	−2.860	0.005

BMI = body mass index; BSA = body surface area; CHD = congenital heart disease; LVEDA = left ventricular end-diastolic area; LVEDD = left ventricular end-diastolic dimension; LVEDV = left ventricular end-diastolic volume; LVEF = left ventricular ejection fraction; LVESD = left ventricular end-diastolic dimension; LVESV = left ventricular end-systolic volume; LVPO = CHD involving left ventricle pressure overload (including aortic stenosis, aortic coarctation, and bicuspid aortic valve); LVSV = left ventricular stroke volume; LVVO = CHD involving left ventricular volume overload (including ventricular septal defect, atrioventricular septal defect, patent ductus arteriosus, and aorto-pumonary window); -i = indexed to BSA.

width/LVEDA increased with increasing body weight whereas it decreased with increasing body height, BMI, LVEDAi, and LVEDDi. Furthermore, the group of neonates was associated with larger vortex height/LVEDA and width/LVEDA.

The sphericity index increased with increasing LV end-systolic volume indexed to BSA (LVESVi), LV stroke volume indexed to BSA (LVSVi), and LV end-systolic dimension indexed to BSA (LVESDi), whereas it decreased with increasing LV end-diastolic volume indexed to BSA (LVEDVi). Finally, vortex area/LVEDA increased with increasing body weight and LVEDAi while it decreased with increasing BMI, BSA, and LVEDDi.

3.5. Reproducibility

The reproducibility for vortex's area measurements was excellent. The intra-rater ICC was 0.96 (95% confidence interval 0.79–0.99) in healthy children and 0.98 (95% confidence interval 0.92–0.98) in children with CHD. The inter-rater ICC were 0.93 (95% confidence interval 0.85–0.97) and 0.97 (95% confidence interval 0.94–0.99), respectively (see Fig. 2).

4. Discussion

This study reports data on LV vortices obtained through high-frame rate BST echocardiography in healthy children and children with CHD. We found that the feasibility of vortex imaging was high in our cohort. After propensity matching, there was no overall significant differences in vortex position and dimensions between both groups. However, significant associations of LV volumes and dimensions with vortex characteristics were found. Furthermore, some subtypes of CHD were associated with changes in vortex position. Our data suggest that the analysis of LV vortices could yield diagnostic and prognostic value and could contribute to our unfolding understanding of the physiology of intracardiac flow in health and disease.

4.1. Vortex imaging in children

Data on vortex imaging in children are limited and previous studies have usually included small samples.[1–6,8] Collins *et al.*[3] performed contrast agent free vector flow imaging in two pigs and two children, each consisting of one subject with CHD, and confirmed that this technique was feasible within a penetration depth of 6.5 cm and able to visualize abnormalities in intracardiac flow. In a preliminary pictorial study, Hansen *et al.*[8]used the technique in 12 healthy newborns and 3 infants with CHD, revealing unique flow patterns in the latter. Although they reported "a pattern as in the healthy newborns, i.e. a jet along the free wall to the apex returning along the septum to the LVOT" – suggesting an LV vortex – the characteristics of this feature were not investigated in detail. Nyrnes *et al.*[4] confirmed feasibility of the technique, showing a good correlation (r = 0.95) of velocity estimates by BST with phantom data and a clinical feasibility of >99% in 102 subjects including 47 children with various cardiac diseases. Subsequent studies have tried to identify distinct intracardiac flow patterns in patients with CHD.[2,5,6]

Data specifically on LV vortex formation in children are limited. In a recent study of 50 preterm infants referred for echocardiography, de Waal et al.[1] performed vortex analysis on BST images and found that LV vortices formed mainly throughout diastole and that peak vortex formation occurred at 87% of the cardiac cycle. Furthermore, they found significant correlations of vortex area with LV dimensions and volumes. Data of LV vortex imaging in children with CHD are lacking.

4.2. Vortex characteristics in health and disease

In our cohort ranging from ages 1 day to 15 years, we found that visualization of clean-edged LV vortices was feasible of about 95% in both healthy children and in those with CHD. The analysis was as fast as conventional color Doppler, requiring not more than 30–60 s for each study. We confirmed previous observations that the main vortex forms almost exclusively during diastole and at the level of the mid-septal region of the LV (at a distance of 40% from the apex and 35% from the IVS).[1]

The differences in vortex characteristics reported in our unmatched analyses were most likely related to the younger age of children with CHD in our cohort and their subsequent smaller cardiac dimensions, as all disappeared after propensity matching. This is in accordance with preliminary reports that found no overall difference in vortex morphology in healthy children and those with CHD, although they differ from data in adults with CHD.[1,7,8,13] Lampropoulos *et al.*[13] found that 9 adults with a Fontan circulation (mean age 31.5 ± 12 years), height and sphericity index of the vortex in the systemic ventricle were significantly smaller whereas vortex width was larger when compared to 15 age-matched controls. Similar findings were also reported in 15 adult patients with abnormal LV systolic function (mean age 52 ± 18 years).[14] In contrast, vortex height and area were increased in 20 adults with dilated cardiomyopathy.[15] Interestingly, the latter study revealed that the observed flow characteristics were

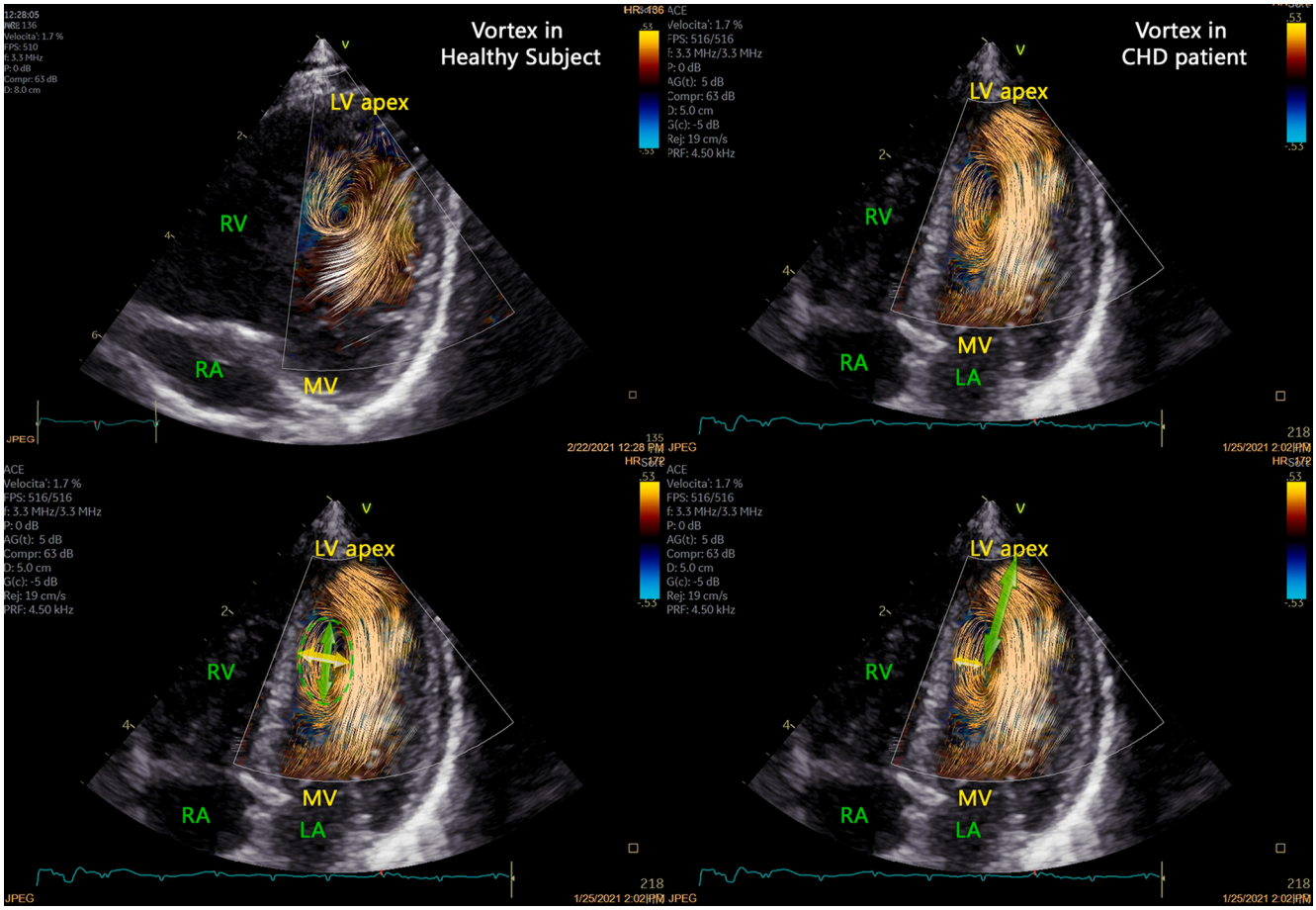

Fig. 2. High-frame rate blood speckle tracking echocardiography of left ventricular vortices in healthy subjects (left) and in CHD patients (right). The lower panels demonstrate the main vortex characteristics: the lower left panel shows vortex dimensions, including height, width, and area; whereas the lower right panel shows vortex position, including distance to the apex and distance to the IVS. CHD = congenital heart disease; IVS = interventricular septum; LA = left atrium; LV = left ventricular; MV = mitral valve; RA = right atrium; RV = right ventricle.

associated with decreased LVEF and increased energy dissipation.

Thus, findings from the present study and previous research seem to suggest that changes in vortex characteristics might only occur in more advanced cardiac dysfunction. Of note, none of the patients included in our cohort had systolic dysfunction. It has been proposed previously that vortices facilitate LV filling and are therefore crucial for efficient ejection of blood through the LVOT.[2,16] Previous studies have indeed shown that vortices represent reservoirs of kinetic energy, and that increased energy dissipation is present in various types of ventricular dysfunction, suggesting that extra effort is required to maintain adequate pump efficiency.[17]

As evidenced in our present study, vortex characteristics were independently associated with LV morphology. The vortex position was found to shift away from the IVS in the overall group of CHDs, while neonates and children with LVPO or LVVO had vortices closer to the IVS. Furthermore, it was found that vortex height/LVEDA, width/LVEDA, and area/LVEDA all decreased with increasing LVEDAi and LVEDDi. This is in accordance with previous biomechanical studies which demonstrated that reducing end-diastolic volumes in a physical left heart simulator led to increased size and dynamics of the LV vortex.[18] In addition, our study found that sphericity index increased with decreasing LVEDVi, suggesting that the vortex became more long-stretched once the ventricle was smaller. Together, these findings suggest that LV shape and internal volume play a critical role in determining vortex dimensions and dynamics, potentially due to the increased confinement associated with smaller intraventricular volumes. The increased vortex dynamics might in that case represent a compensatory mechanism to maintain cardiac output. In this regard, it is relevant that our regression models revealed larger vortex height/LVEDA and width/LVEDA in neonates, where distinct patterns of contractility, preload, and afterload have been described.[19]

An important question remains what role vortex imaging could play in the diagnosis and prognostication of children with cardiac disease. As suggested above, currently, vortices only seem to show distinct features once cardiac dysfunction is also evident based on conventional echocardiographic measurements. However, with improved detection of subtle changes in vortex characteristics and better techniques to quantify energy dissipation, vortices might become potential preclinical predictors of clinical deterioration in the future. The study of intracardiac vortices might improve upon current measures for prognostication. In this regard, it has been shown that kinetic energy fluctuation, a measure of the degree of regularity in flow or turbulence, serves as an independent predictor for major adverse cardiac events in patients with congestive heart failure and systolic dysfunction.[17]

5. Limitations

Despite the large sample size and wide range of complex types of CHD included in the present study, there are some limitations that merit consideration. First, the numbers of patients with RVVO, TGA, or other types of CHD were low, thus limiting our ability to identify associations of these conditions with vortex characteristics. Second, all included subjects had normal LV systolic function, such that the present study could not investigate vortex characteristics in systolic dysfunction. In

addition, we did not evaluate diastolic patterns, which are difficult to classify in the pediatric population and especially at lower ages.[20,21] Since we dd not collected diastolic parameters we could not obtain the vortex formation time.[22] Third, the software that we employed did allow for quantitative measures of vorticity, energy loss, and kinetic energy.[2] Furthermore, due to current technical limitations, we were unable to visualized the main vortex along all the different phases of the cardiac cycle for all patients, and the visualization of more than one vortex was only possible in 9 healthy subjects (7.6%) and 7 children with CHDs (16.3%). The plane wave transmit technology has a reduced penetration and is currently reserved only for higher frequency probes with limited shallow depths, thus limiting application in older children. Finally, blood flow tracking is not available in real-time during live scanning, although postprocessing can be done directly on the echograph and requires just a few seconds.

6. Conclusion

Presenting data from a large cohort with a wide range of ages and including various types of CHD, the present study demonstrated feasibility of LV vortex analysis using high-frame rate BST echocardiography in children. Vortex characteristics were significantly associated with LV volumes and dimensions and were modified in some types of CHD, suggesting potential diagnostic and prognostic implications. Therefore, the study of vortices might add to our understanding of intracardiac flow in the pediatric population. Future studies are warranted to further establish applications of vortex imaging during routine clinical evaluation of children with CHD.

Declaration of Competing Interest

The authors declare the following financial interests/personal relationships which may be considered as potential competing interests: S. Kutty is consultant for GE Healthcare. All other authors declare that they have no competing interests.

Acknowledgement

J. Van den Eynde was supported by a Fellowship of the Belgian American Educational Foundation.

Funding

None.

Appendix A. Supplementary material

Supplementary data to this article can be found online at https://doi.org/10.1016/j.ijcha.2021.100897.

References

[1] K. de Waal, E. Crendal, A. Boyle, Left ventricular vortex formation in preterm infants assessed by blood speckle imaging, Echocardiography. 36 (2019), 1364 71.
[2] O. Villeman, J. Baranger, M.K. Friedberg, C. Papadacci, A. Dizeux, E. Messas, et al., Ultrafast Ultrasound Imaging in Pediatric and Adult Cardiology: Techniques, Applications, and Perspectives, JACC Cardiovasc. Imag. 13 (2020) 1771–1791.
[3] R.T. Collins II, M.E. Laughlin, S.M. Lang, E.H. Bolin, J.A. Daily, H.A. Jensen, M. O. Jensen, Real Time Transthoracic Vector Flow Imaging of the Heart in Pediatric Patients, Prog Pediat Cardiol. 53 (2019) 28–36.
[4] S.A. Nyrnes, S. Fadnes, M.S. Wigen, L. Mertens, L. Lovstakken, Blood Speckle-Tracking Based on High-Frame Rate Ultrasound Imaging in Pediatric Cardiology, J. Am. Soc. Echocardiogr. 33 (4) (2020) 493–503.e5.
[5] M. Cantinotti, P. Marchese, M. Koestenberger, R. Giordano, G. Santoro, N. Assanta, S. Kutty, Intracardiac Flow Visualization Using High-Frame Rate Blood Speckle Tracking Echocardiography: Illustrations from infants with Congenital Heart Disease, Echocardiography. 38 (4) (2021) 707–715, https://doi.org/10.1111/echo.v38.410.1111/echo.15009.
[6] N. Borrelli, M. Avesani, J. Sabatino, et al., Blood speckle imaging: A new echocardiographic approach to study fluid dynamics in congenital heart disease, Int. J. Cardiol. 2 (2021), 100079.
[7] H. Abe, G. Caracciolo, A. Kheradvar, G. Pedrizetti, B.K. Khandheria, J. Narula, P. P. Sengputa, Contrast echocardiography for assessing left ventricular vortex strength in heart failure: a prospective cohort study, Eur. Heart J. Cardiovasc. Imag. 14 (2013) 1049–1060.
[8] Kristoffer Hansen, Klaus Juul, Hasse Møller-Sørensen, Jens Nilsson, Jørgen Jensen, Michael Nielsen, Pediatric Transthoracic Cardiac Vector Flow Imaging – A Preliminary Pictorial Study, Ultrasound Int. Open. 05 (01) (2019) E20–E26.
[9] M. Cantinotti, M. Scalese, R. Giordano, E. Franchi, P. Marchese, N. Assanta, et al., Three-Dimensional Echocardiography Derived Nomograms for Left Ventricular Volumes in Healthy Caucasian Italian Children, J. Am. Soc. Echocardiogr. 32 (2019) 794–797.
[10] Roberto M. Lang, Luigi P. Badano, Victor Mor-Avi, Jonathan Afilalo, Anderson Armstrong, Laura Ernande, Frank A. Flachskampf, Elyse Foster, Steven A. Goldstein, Tatiana Kuznetsova, Patrizio Lancellotti, Denisa Muraru, Michael H. Picard, Ernst R. Rietzschel, Lawrence Rudski, Kirk T. Spencer, Wendy Tsang, Jens-Uwe Voigt, Recommendations for cardiac chamber quantification by echocardiography in adults: an update from the American Society of Echocardiography and the European Association of Cardiovascular Imaging, J. Am. Soc. Echocardiogr. 28 (1) (2015) 1–39.e14.
[11] Massimiliano Cantinotti, Raffaele Giordano, Marco Scalese, Sabrina Molinaro, Bruno Murzi, Nadia Assanta, Maura Crocetti, Marco Marotta, Sergio Ghione, Giorgio Iervasi, Strengths and limitations of current pediatric blood pressure nomograms: a global overview with a special emphasis on regional differences in neonates and infants, Hypertens. Res. 38 (9) (2015) 577–587.
[12] George B. Haycock, George J. Schwartz, David H. Wisotsky, Geometric method for measuring body surface area: a height-weight formula validated in infants, children, and adults, J. Pediatr. 93 (1) (1978) 62–66.
[13] K. Lampropoulos, W. Budts, A. Van de Bruaene, E. Troost, J.P. van Melle, Visualization of the intracavitary blood flow in systemic ventricles of Fontan patients by contrast echocardiography using particle image velocimetry, Cardiovasc Ultrasound. 10 (2012) 5, https://doi.org/10.1186/1476-7120-10-5.
[14] Geu-Ru Hong, Gianni Pedrizzetti, Giovanni Tonti, Peng Li, Zhao Wei, Jin Kyung Kim, Abinav Baweja, Shizhen Liu, Namsik Chung, Helene Houle, Jagat Narula, Mani A. Vannan, Characterization and quantification of vortex flow in the human left ventricle by contrast echocardiography using vector particle image velocimetry, JACC Cardiovasc. Imag. 1 (6) (2008) 705–717.
[15] Chouchou Tang, Yizhong Zhu, Jing Zhang, Chengcheng Niu, Dan Liu, Yacong Liao, Lijun Zhu, Qinghai Peng, Analysis of left ventricular fluid dynamics in dilated cardiomyopathy by echocardiographic particle image velocimetry, Echocardiography. 35 (1) (2018) 56–63.
[16] A. Kheradvar, C. Rickers, D. Morisawa, M. Kim, G.R. Hong, G. Pedrizzetti, Diagnostic and prognostic significance of cardiovascular vortex formation, J. Cardiol. 74 (5) (2019 Nov) 403–411, https://doi.org/10.1016/j.jjcc.2019.05.005. Epub 2019 Jun 26.
[17] I.C. Kim, G.R. Hong, Intraventricular Flow: More than Pretty Pictures, Heart Fail Clin. 15 (2) (2019 Apr) 257–265, https://doi.org/10.1016/j.hfc.2018.12.005.
[18] M. Samaee, N. Nelsen, M. Gaddam, A. Santhanakrishnan, Diastolic Vortex Alterations with Reducing Left Ventricular Volume: An in Vitro Study, J. Biomech. Eng. (2020 Jun 30), https://doi.org/10.1115/1.4047663.
[19] D.G. Rowland, H.P. Gutgesell, Noninvasive assessment of myocardial contractility, preload, and afterload in healthy newborn infants, 818 21, Am. J. Cardiol. 75 (12) (1995 Apr 15), https://doi.org/10.1016/s0002-9149(99)80419-6.
[20] M. Cantinotti, L. Lopez, Nomograms for blood flow and tissue Doppler velocities to evaluate diastolic function in children: a critical review, J. Am. Soc. Echocardiogr. 26 (2013), 126 41.
[21] Andreea Dragulescu, Luc Mertens, Mark K. Friedberg, Interpretation of Left Ventricular Diastolic Dysfunction in Children With Cardiomyopathy by Echocardiography, Circ Cardiovasc Imaging. 6 (2) (2013) 254–261.
[22] Aparna Kulkarni, Daisuke Morisawa, Daisy Gonzalez, Arash Kheradvar, Kheradvar A Age-related changes in diastolic function in children: Echocardiographic association with vortex formation time, Echocardiograph 36 (10) (2019) 1869–1875.